Journal of Zhejiang University-SCIENCE A (Applied Physics & Engineering)
ISSN 1673-565X (Print); ISSN 1862-1775 (Online)
www.zju.edu.cn/jzus; www.springerlink.com
E-mail: jzus@zju.edu.cn

A weather research and forecasting model evaluation for simulating heavy precipitation over the downstream area of the Yalong River Basin*

Ming-xiang YANG[†1,2], Yun-zhong JIANG[†‡2], Xing LU[3], Hong-li ZHAO[2], Yun-tao YE[2], Yu TIAN[2]

([1]*Department of Hydraulic Engineering, Tsinghua University, Beijing 100084, China*)

([2]*State Key Laboratory of Simulation and Regulation of Water Cycle in River Basin, China Institute of Water Resources and Hydropower Research, Beijing 100038, China*)

([3]*China Eastern Route Corporation of South-to-North Water Diversion, Beijing 100038, China*)

[†]E-mail: yangmx12@mails.tsinghua.edu.cn; larkking@sina.com

Received Nov. 24, 2014; Revision accepted Dec. 2, 2014; Crosschecked Dec. 26, 2014

Abstract: The forecasting capability of the weather research and forecasting (WRF) model for heavy precipitation in the downstream area of the Yalong River Basin in Southwest China was evaluated for the first time through the simulation of three heavy precipitation events with seven commonly used microphysics parameterization schemes (MPS) (Kessler, Lin *et al.* (Lin), Single-Moment 3-class (WSM3), Single-Moment 5-class (WSM5), Ferrier, Single-Moment 6-class (WSM6), and New Thompson *et al.* (NTH)) and three cumulus parameterization schemes (CPS) (Kain-Fritsch (KF), Betts-Miller-Janjic (BMJ), and Grell-Devenyi (GD)). Of the three rainfall events, the first two are typical large-area heavy precipitation events in the Yalong River Basin and consist of several continuous storms. The third one is a heavy precipitation event with only one storm. In this study, a triple nested domain with a 3-km grid resolution inner-most domain over the study area was configured for the WRF model. We employed the probability of detection (POD), false alarm ratio (FAR), BIAS, and equitable threat (ET) scores to compare the spatial distribution of heavy rainfall created by the WRF model with the observations from the gauges in the downstream area of the river basin. The root mean squared errors (RMSEs) at each sub river basin and the whole downstream of Yalong River Basin were also calculated for the evaluation. In addition, it is important to include the computation efficiency when choosing a scheme combination. We recorded the time consumption for each model simulation and made comparisons for selecting the optimum scheme with less time consumption and acceptable prediction accuracy. Through comprehensive comparison, the scheme combination of WSM3 and GD holds a stable performance in leveraging the prediction accuracy and computation efficiency for the heavy precipitation events.

Key words: Weather research and forecasting (WRF) model, Yalong River Basin, Heavy precipitation, Precipitation simulation, Precipitation verification, Cumulus parameterization scheme, Microphysics scheme

doi:10.1631/jzus.A1400347 **Document code:** A **CLC number:** P457.6

1 Introduction

The Yalong River (26°32′ N–33°58′ N, 96°52′ E–102°48′ E) is a 1323 km long river with a total catchment area of about 130000 km^2 in Sichuan Province in Southwest China. As a tributary of the Yangtze River, it originates from the Bayan Har Mountain Group in the southeast of Qinghai Province, and is merged into the Yangtze River in

‡ Corresponding author

* Project supported by the National Natural Science Foundation of China (Nos. 51109177 and 51209223), the Major National Science and Technology Program (No. 2012ZX07205-005), the National Key Technology R&D Program of China during the "12th Five-Year Plan" (No. 2013BAB05B01), and the Doctoral Thesis Innovation Program of the China Institute of Water Resources and Hydropower Research

ORCID: Ming-xiang YANG, http://orcid.org/0000-0002-6085-6762; Yun-zhong JIANG, http://orcid.org/0000-0002-9918-2670

Panzhihua City in the southwest of Sichuan Province. In the downstream area of the Yalong River Basin, the Hengduan Mountains provides an average elevation of more than 2000 m, which strongly affects the local weather and precipitation. The Yalong River Basin is mainly affected by the monsoon climate and the local water vapor primarily comes from the Bengal Bay, the South China Sea, and the Beibu Bay. Most precipitation occurs in the period from May to October and shows an increasing trend from the northwest to southeast. In the Yalong River Basin, the damaging floods occur immediately after the heavy rainfall and primarily in the summer and always leads to huge losses of life and property.

In addition to the heavy precipitation and flood disaster, the Yalong River Basin is well known as one of the most important electricity production basins in the 12 hydropower areas in China (Jia *et al.*, 2004). Several large hydroelectric power stations have been built in the river basin, including the famous Ertan Hydroelectric Power Station in the downstream area of the river, near the city of Panzhihua (Peng *et al.*, 2011). As the river flow prediction is very important for flood control and the operation of the hydroelectric power stations, the hydrologic models for the Yalong River Basin have been widely studied, including the distributed hydrologic models (Zhou *et al.*, 2009). In the distributed hydrologic models, the rainfall data with the highest temporal-spatial resolution are required for the prediction of water flow. However, the precipitation observed by the rain gauges of the Yalong River Basin could not provide the data with a high enough resolution for the distributed hydrological models because of the sparse rain gauge network. In recent years, with the development in computing and observation technologies, the resolution of numerical weather prediction (NWP) models has become more precise and can meet the requirements for the distributed hydrologic models. Many scientists began to use NWP outputs as the inputs of the distributed hydrologic models to predict a flood. However, the most important concern before combining an NWP model with a hydrologic model for predicting the basin flood is to evaluate the NWP model's capability in simulating the spatial distribution of heavy rainfall and the total precipitation amounts over the river basin (Pennelly *et al.*, 2014). The weather research & forecasting (WRF) model, as one of the most advanced NWP models, was mainly employed in mesoscale rainfall forecasting and research, and could provide the required resolution for the distributed hydrological models. Hong and Lee (2009), Dodla and Ratna (2010), Mastrangelo *et al.* (2011), and Dodla and Desamsetti (2014) used WRF models to study the heavy rainfall systems and attempted to disclose the mechanisms of disastrous weather events.

In NWP models, cloud microphysics parameterization schemes (MPS) are adopted to resolve the processes of rain production, falling, and evaporation. Cumulus parameterization schemes (CPS) are often used when the individual model grid size is so large that it cannot show the effects of the cumulus clouds. Since the simulated total precipitation amounts in the NWP models are largely determined by the combination of CPS and MPS, it is very important to analyze the performances of the CPS and MPS before any hydrological application in the study area (Wang and Seaman, 1997; Fiori *et al.*, 2011; Cossu and Hocke, 2013). Kerkhoven *et al.* (2006) selected five CPS in an MM5 model to analyze their performances in the simulation of a summer monsoon in China and found that the Grell scheme was the most robust and showed the best performance at various precipitation intensity levels. Pennelly *et al.* (2014) used five different CPS to simulate three storms for obtaining the optimum schemes and found that the Kain-Fritsch (KF) and explicit CPS were the most accurate ones. Wang *et al.* (2011) and Litta *et al.* (2012) also found that the Grell scheme and KF scheme performed well in their research work. Alam *et al.* (2014) used six different MPS and two different CPS to simulate a heavy precipitation event in Bangladesh and found that the Single-Moment 6-class (WSM6) and KF combination gave a better simulation result. Chandrasekar and Balaji (2012) conducted two experiments to find out the optimum physics schemes for the precipitation simulation and the results showed that the best set of physics schemes performed better than the default schemes.

In general, the finer spatial resolution of the NWP model grid allows more accurate results (Wang

and Seaman, 1997; Done *et al.*, 2004). However, the model simulation with the finer resolution will always require much more time. Considering the large study area, we chose a grid resolution of 3 km to get the balance between prediction accuracy and time consumption. Besides the domain settings, the time consumption of the model is mainly related to the chosen MPS. In our study, the time consumption was recorded for selecting the schemes with less time consumption and more acceptable prediction accuracy.

Three heavy rainfall events over the study area were simulated with a WRF model: Event A from Sept. 22 to Sept. 27, 2005, Event B from July 7 to July 11, 2005, and Event C from June 27 to June 29, 2006.

Event A lasted more than 5 d and covered a large area, showing a typical condition for heavy precipitation over the Yalong River Basin. At about 00 UTC on Sept. 22, 2005, a low pressure center together with a northwest upper airflow arose near Xichang City in the southeast of the study area and the near saturated water vapor provided a favorable condition for heavy precipitation. The largest 24-h precipitation amount of 123.8 mm was recorded on Sept. 25 at the Abili Rain Gauge Station. During this precipitation, a flood occurred in the sub 3 area (Anning River, observed by the Wantan Station), its flood peak reached 1270 m^3/s which accounted for about one third of the mainstream discharge (3960 m^3/s).

Event B was affected by the edge of a subtropical high pressure belt, contained several convective systems, and lasted for 4 d from July 7, 2005 to July 11, 2005. The heaviest rainfall was observed at the Puwei Rain Gauge Station and the 24-h accumulated rainfall reached 57 mm. This heavy precipitation produced a flood peak of 5960 m^3/s at the Xiaodeshi Station from rainfall of 1560 m^3/s in just 2 d.

A third simulation case (Event C) was added to give an example of a short and regional rainfall that also caused disasters. Event C represented a heavy rainfall case only containing a single storm with a total precipitation amount of less than those for Event A and Event B over the river basin. Event C occurred from June 27 to June 29, 2006 and the maximum 24-h rainfall of 62.7 mm was recorded at the Jinhe Rain Gauge Station. The main difference between Event C and the previous two events is that it consists of only one significant storm in the study period over the downstream area of the Yalong River Basin from the northeast to southwest. Although the total precipitation amount of Event C is much less than those of Event A and Event B, it can also cause geological disasters such as mudslides from the intense precipitation within a short period of time. Event C caused a catastrophic mudslide with 3 people killed, 38 people missing and with the local power grids failing in Ningnan. Thus, it is important to include Event C in this study for developing a disaster warning.

One purpose of this work is to evaluate the capability of WRF to simulate the heavy precipitation in the downstream area of the Yalong River Basin before applying the WRF model for basin flood prediction. Another is to determine the optimum combination of the MPS and CPS for a model grid resolution of 3 km for developing an application in forecasting runs. A comparison between the precipitation simulated by WRF model and the precipitation observed by rain gauges was carried out across the downstream area of the Yalong River Basin as well as the individual sub-basin to examine the accuracy of rainfall locations and precipitation amounts. Furthermore, we investigated the time consumption of each case which is important when the computing resource is limited or the simulation period is fairly long.

In the paper, the optimal scheme of a WRF model for the application in the Yalong River Basin was studied for the first time for the prediction of the basin precipitation and runoff flow using a finer scale. The computation time was included as one index in the evaluation of the prediction performance as well, which was seldom considered in previous related studies.

2 NWP model description and evaluation dataset

2.1 WRF model

As one of the most advanced NWP models, the WRF model is designed to replace the MM5 model. The WRF model can serve as the operation model or the scientific research model (Michalakes *et al.*, 1999;

Skamarock *et al.*, 2008) because of its two different cores. While the advanced research WRF (ARW) core is designed for atmospheric research, the non-hydrostatic mesoscale model (NMM) core is developed for operational forecasting. More details are available from the Online Tutorial (http://www2.mmm.ucar.edu/wrf/OnLineTutorial/).

In this study, we employed the ARW core of the WRF model version 3.5 to estimate the capability to simulate heavy precipitation over the downstream area of the Yalong River Basin. The WRF model domain in this study contained three one-way nested grids (Fig. 1). First, the outer Domain 1 covered the major part of Southeast Asia with a coarse grid resolution of 27 km. Second, the middle Domain 2 was set to cover the large part of Southwest China with a finer grid resolution of 9 km. Finally, the inner Domain 3 covered the whole Yalong River Basin to adequately represent the weather system of the study region with a very high grid resolution of 3 km. Thirty-five layers were set in the vertical direction with 50 hPa as the top pressure. In order to get a stable model, we set a 24-h spin-up running period before the first day of each heavy rainfall event. The initial and boundary conditions were determined by the National Centers for Environmental Prediction (NCEP) Final Analyses (FNL) data with a grid resolution of 1°. In addition, the update interval of the boundary conditions was set to be 6 h. The details of the WRF configuration are given in Table 1.

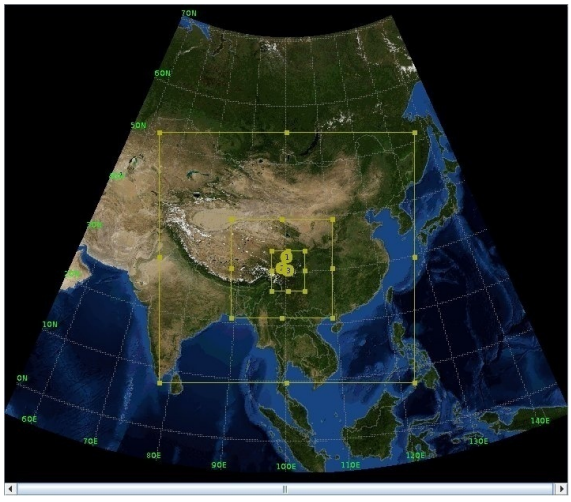

Fig. 1 Domains set in the WRF model
The WRF domain consists of three nested domains: Domain 1 with a grid resolution of 27 km, Domain 2 with a grid resolution of 9 km, and Domain 3 with a grid resolution of 3 km

The MPS of the WRF model is designed to describe the cloud and precipitation processes, while the CPS is used to describe the sub-grid cloud and precipitation processes that are too fine to be resolved by

Table 1 Overview of WRF model configurations

Dynamics	Non-hydrostatic
Starting time	Event A: 00 UTC Sept. 21, 2005; Event B: 00 UTC July 6, 2005; Event C: 00 UTC June 24, 2006
Ending time	Event A: 00 UTC Sept. 27, 2005; Event B: 00 UTC July 11, 2005; Event C: 00 UTC July 1, 2006
Interval	6 h
Grid size	Domain 1: (203×199)×35; Domain 2: (241×235)×35; Domain 3: (241×289)×35
Resolutions	Domain 1: 27 km×27 km; Domain 2: 9 km×9 km; Domain 3: 3 km×3 km
Covered area	26.5° N–34° N and 97° E–104° E
Map projection	Mercator
Horizontal grid system	Arakawa-C grid
Time step	90 s
Vertical coordinates	Terrain-following hydrostatic pressure; vertical coordinate with 35 vertical levels
Time integration scheme	3rd order Runga-Kutta scheme
Spatial differencing scheme	6th order center differencing
Planetary boundary layer (PBL) scheme	Yonsei University scheme (YSU)
Microphysics	Kessler scheme (Kessler); Lin *et al.* scheme (Lin); Single-Moment 3-class scheme (WSM3); Single-Moment 5-class scheme (WSM5); Ferrier scheme (Ferrier); Single-Moment 6-class scheme (WSM6); New Thompson *et al.* scheme (NTH)
Cumulus parameterization*	Kain-Fritisch (KF); Betts-Miller-Janjic (BMJ); Grell-Devenyi (GD)
Surface layer parameterization	Noah land surface scheme
Longwave radiation	Rapid radiative transfer model (RRTM)
Shortwave radiation	Dudhia scheme

* Only set in Domains 1 and 2

the model. All the schemes significantly affect the total precipitation amount and the rainfall distribution. In order to estimate the prediction capability of the WRF model for the precipitation in the downstream area of the Yalong River Basin and determine the optimum combination of MPS and CPS, we used seven different MPS and three different CPS (only set in Domain 1 and Domain 2) to simulate the Events A, B, and C.

2.1.1 Microphysics parameterization schemes

As shown in Table 1, the selected schemes are the Kessler scheme, Lin *et al.* (Lin) scheme, Single-Moment 3-class (WSM3) scheme, Single-Moment 5-class (WSM5) scheme, Ferrier scheme, WSM6 scheme, and the New Thompson *et al.* (NTH) scheme.

The Kessler scheme is the oldest MPS in WRF. The Kessler scheme (Kessler, 1995), which was taken from COMMAS (Wicker and Wilhelmson, 1995), is a simple warm cloud scheme and it includes water vapor, cloud water, and rain. The Lin (Lin *et al.*, 1983) scheme has water vapor, cloud water, rain, cloud ice, snow and graupel included in it, and is a relatively sophisticated MPS. Lin is a commonly used scheme for various research applications (Evans *et al.*, 2012). The WSM3 scheme (Hong *et al.*, 2004) is based on the old NCEP3, and it can predict cloud water/ice, vapor and rain/snow. The WSM3 scheme distinguishes cloud water and rain from cloud ice and snow through judging whether the temperature is above or below freezing. As a more complex version of WSM3, WSM5 stores different states of cloud water and precipitation separately, and also includes the supercooled water. The WSM6 scheme (Hong and Lim, 2006) is an extension of WSM5 with additional processes related to graupel (Lin *et al.*, 1983) being added. It has the maxing ratios of water vapor, cloud water, cloud ice, snow, rain, and graupel. The Ferrier scheme (Ferrier *et al.*, 2002), also known as the Eta-Ferrier scheme, is commonly used in NWP models for its good computing performance. The Ferrier scheme predicts cloud water, rain, cloud ice, and precipitation ice. The precipitation ice can be in the form of snow, graupel or frozen raindrops based on the density information expected from a local array (Alam, 2014). The NTH scheme (Thompson *et al.*, 2004) includes a concentration analysis for ice, and was developed to predict the freezing drizzle events for aircraft. It (Thompson *et al.*, 2004) uses look-up tables to describe the size distribution of the hydrometeors. In the WRF model version 3.5, the NTH scheme is the most sophisticated MPS, and its computational efficiency is relatively lower than those of other MPS for its sophisticated structure.

2.1.2 Cumulus parameterization schemes

The three different CPS, namely, KF (Kain, 2004), Betts-Miller-Janjic (BMJ) (Betts and Miller, 1986), and Grell-Devenyi (GD) (Grell and Devenyi, 2002), were chosen for the present study for combining with seven different MPS.

The KF scheme (Kain and Fritsch, 1990) is an extension of the earlier Fitsch-Chappell scheme (Fritsch and Chappell, 1980), and uses a simple cloud model. It incorporates a trigger function and assumes that the precipitation will happen when the condensation amount in the updraft exceeds the threshold value. Much more details can be found in (Kain, 2004). The BMJ scheme is based on the Betts-Miller scheme (Betts and Miller, 1986) with some modifications. It is triggered when an instability cloud depth is higher than 200 hPa. The BMJ scheme was considered to be robust in other studies and was an operational scheme at NCEP (Pennelly *et al.*, 2014). The GD scheme is known as an ensemble cumulus scheme (Grell and Devenyi, 2002), and while the trigger function varies for each member it is commonly based on convective available potential energy (CAPE), CAPE trend, and moisture convergence. As a result of the ensemble methodology, the GD scheme performed well at the higher grid resolution, in addition to when utilizing it with coarse mesh (Skamarock *et al.*, 2008).

At 3 km resolution, most storm dynamics are resolvable and there is no need to invoke a CPS. So the CPS was only used in outer Domain 1 and Domain 2. It is important to note that even with the explicit CPS in Domain 3, different CPS in the two outer domains will change the rainfall amounts and the distribution of the precipitation in Domain 3.

2.2 Observation data

The observation data of precipitation for the evaluation were from the Yalong River Hydropower Development Company (http://www.ehdc.com.cn/faces/en/overview2.html). Rain gauge observations

from 51 meteorological stations in the downstream area of the Yalong River Basin were used to evaluate the outputs of the WRF model. The distribution of stations and six sub-river basins are shown in Fig. 2. Inevitably, there will be a representativeness error caused by the mismatching between the high-resolution WRF model output data and the low-resolution observation data. Because the error sometimes has a significant effect on the evaluation results (Tustison *et al.*, 2001; Benedetti *et al.*, 2005), we estimated the prediction capability of the model in several aspects, including the precipitation distribution across the study area, the total precipitation amount, and the precipitation at the observation point. To evaluate the precipitation in a river basin, the Cressman algorithm (Cressman, 1959) was used to interpolate the observation data into the model grid points to get the precipitation amount of a certain sub-basin or the entire downstream river basin. Moreover, the model grid that spatially contained each rain gauge was taken as the comparison object in the observation point evaluation.

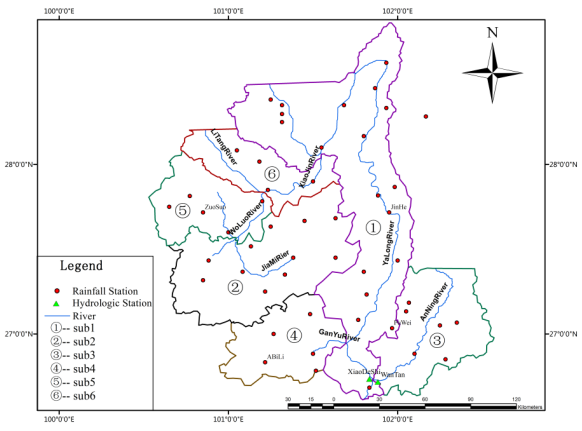

Fig. 2 Sub river basins in the downstream area of the Yalong River
Filled circles indicate the positions of the rain gauges

3 Evaluation methodology

The accurate prediction of the precipitation amount over the sub river basins and the amounts at the station points are very important in the operation of hydrologic forecasting. The simulated precipitation was evaluated in two different ways, namely the evaluation of the total precipitation over the river basin and the observation point evaluation. In addition, the computational efficiency of different schemes was evaluated, and the evaluation results could be used as an important reference when the computing resource is limited.

3.1 Evaluation of total precipitation over the river basin

To calculate the average root mean squared error (RMSE) (Shamim *et al.*, 2012) at the sub-basins and the whole study area (the downstream area of the Yalong River Basin), the total precipitation simulated by the WRF model at each grid point was compared to the total observed precipitation amount interpolated at the corresponding grid point.

The RMSE is calculated according to

$$\mathrm{RMSE}=\sqrt{(1/N)\sum_1^N (S-O)^2}, \tag{1}$$

where S is the precipitation amount of the individual grid point simulated by the WRF model, O is the interpolated observed precipitation amount at the same grid point, and N is the total number of the grid points.

The percentage of the simulated precipitation over the observed precipitation was also calculated for further evaluation of the distribution of the precipitation over the sub-basins and the whole study area. The percentage can directly provide the information of overestimation or underestimation of the precipitation amounts simulated by different parameterization schemes of microphysics and cumulus, while the RMSE allows a general evaluation on the accuracy of WRF simulation across the sub-basins or the whole study area.

3.2 Evaluation at observation point

In order to fully evaluate the WRF prediction capability, we also directly compared the simulated precipitation amounts with the observation values from 51 rain gauge stations. In the evaluation of the total precipitation over the river basin, the interpolated values were used. However, in this method, the daily observations of the rain gauges were compared

with the simulated precipitation, which was extracted from the precipitation field simulated by the WRF model according to the location of the rain gauges. This statistical evaluation was carried out with four indexes at three 24-h rainfall accumulated thresholds: 10 mm, 15 mm, and 25 mm. These four indexes, probability of detection (POD), false alarm ratio (FAR), frequency BIAS score (BIAS), and equitable threat (ET) (Schaefer, 1990), were calculated using a 2×2 contingency table, as shown in Table 2. H represents the number of hits, F represents the number of false alarms, and M represents the number of missing or non-detected events. The statistical score calculation formulas of POD, FAR, BIAS, and ET are provided as follows (Jasper and Kaufmann, 2003; Pennelly *et al.*, 2014):

$$\mathrm{POD}=H/(H+M). \tag{2}$$

$$\mathrm{FAR}=F/(H+F). \tag{3}$$

$$\mathrm{BIAS}=(H+F)/(H+M). \tag{4}$$

$$\mathrm{ET}=(H-E)/(H+M+F-E), \tag{5}$$

where

$$E=(H+F)(H+M)/n, \tag{6}$$

where n is the total number of observation stations.

Table 2 Precipitation contingency table considering observations (obs) and simulations (sim) for a given threshold (th)

Simulated	Observed	
	obs≥th	obs<th
sim≥th	H	F
sim<th	M	NONE

The elements (H, M, F, and NONE) are determined by the number of observation stations whose observed values and simulated values exceed the given rainfall threshold or not. For instance, if the elements are calculated at the threshold of 5 mm and there is an observed value of 7 mm at a rain gauge, H will be increased by one when the simulated value of the rain gauge exceeds 5 mm or M will be increased by one when the simulated value does not exceed 5 mm. The calculation methods of F and NONE are similar to those of H and M

The POD represents the capability of rainfall detection with a score of 1, indicating that the WRF model can correctly simulate all the observed precipitations above the given threshold. FAR is the opposite to POD, and an FAR value of 1 indicates that all the station precipitations are incorrectly simulated by the WRF model. BIAS determines whether the number of stations with a precipitation in the WRF model simulation is more or less than the number of the stations with the observed precipitation. A number of 1 is the dividing line of BIAS. A BIAS value of 1 would indicate that the number of stations with a precipitation in the WRF model simulation is equal to the number of the station with the observed precipitation, whereas a BIAS value below/over 1 would imply that the stations with precipitation in the WRF model simulation was less/more than the stations with the observed precipitation. ET is an evaluation index that represents the overall skill of the simulation capability of the WRF model. An ET score of 1 indicates the perfect simulation, while a value of 0 indicates the same accuracy as a random precipitation simulation.

3.3 Computational efficiency evaluation

Sixty-three simulations were performed for three different precipitation events with seven different MPS and three different CPS. Due to the heavy computing load, the simulations were conducted with a high-performance cluster in the State Key Laboratory of Simulation and Regulation of Water Cycle in the River Basin of IWHR (China Institute of Water Resources and Hydropower Research). The cluster had six nodes and five of them were used. Each node has 2 Intel(R) Xeon(R) CPUs (X5670@2.93 GHz) with 12 cores in each CPU, and there is 94 GB memory and 3 TB storage space for each node. The Red Hat Enterprise version 5.5 operation system was installed in the cluster. In order to obtain the time consumption under the ideal state, all other time-consuming runs were forbidden during the operation of the WRF model.

4 Results and discussion

4.1 Event A

Event A was simulated by the WRF model with seven different MPS and three different CPS. Tables 3–5 recorded the percent simulation of observed (%), RMSE (mm), and computation time (min) of the 21 simulations. As shown in Table 3, the total amounts simulated by the 21 model runs were

different from each other. However, there were some general results which can be summarized from Table 3. The simulations with Kessler, Lin, WSM5, and WSM6 significantly underestimated the precipitation, and they could not reflect the actual situation. When using the CPS KF, BMJ and GD, we found that the simulations with GD produced the most precipitation and BMJ produced the least. Table 4 reflected the similar results as shown in Table 3. Due to the least precipitation being simulated by the model runs with Kessler, the average RMSE values of these were the highest in the seven MPS (Table 4). Table 5 recorded the computation time in minutes of the 21 model runs. From the average computation times of different MPS (last row in Table 5) and CPS (last column in Table 5), we could infer that the computation time of a model simulation was mainly determined by the MPS. In order to get the optimal scheme combinations, we obtained each value in Table 3 subtracted by 100 and took the absolute value, sorted the absolute value and obtained the rankings of the scheme combinations. Similarly, we obtained the rankings of the scheme combinations according to the RMSE values in Table 4. Finally, we obtained the average value of the two rankings of each scheme combination, and took the top five for further comparison. The top five scheme combinations were WSM3 & GD, WSM3 & BMJ, Ferrier & KF, Ferrier & GD, and NTH & GD. Fig. 3 depicts the 6-d total precipitation fields from the observations and the top five simulations. All the five simulations reproduced the major spatial distribution features of the precipitation, and generated the majority of the total precipitation amount in a tongue-shaped area just like the observations. However, there were some differences among the five simulations. Compared with the observations, the WSM3 & GD combination (Fig. 3b) provided a good simulation of the main rainfall field in the south of the study area and the maximum precipitation was in close spatial agreement with the

Table 3 Percent simulation of observed (%) of 21 model runs for Event A with seven different MPS and three different CPS

CPS	Percent simulation of observed (%)							Average
	Kessler	Lin	WSM3	WSM5	Ferrier	WSM6	NTH	
KF	43.8	74.8	87.9	64.3	85.3	61.8	74.6	70.4
BMJ	46.5	52.1	74.3	47.7	71.3	56.6	60.0	58.4
GD	40.8	74.9	86.9	83.5	104.7	82.2	82.2	79.1
Average	43.7	67.3	83.0	65.2	87.1	66.9	72.3	

Table 4 RMSE (mm) of 21 model runs for Event A with seven different MPS and three different CPS

CPS	RMSE							Average
	Kessler	Lin	WSM3	WSM5	Ferrier	WSM6	NTH	
KF	19.5	12.7	12.7	12.3	11.6	12.5	12.3	13.4
BMJ	19.6	13.7	10.6	13.4	12.3	13.0	12.8	13.6
GD	19.2	12.5	10.3	12.3	11.4	12.9	12.0	12.9
Average	19.4	13.0	11.2	12.7	11.8	12.8	12.4	

Table 5 Computation time (min) of 21 model runs for Event A with seven different MPS and three different CPS

CPS	Computation time (min)							Average
	Kessler	Lin	WSM3	WSM5	Ferrier	WSM6	NTH	
KF	519	701	540	616	579	683	771	630
BMJ	520	705	533	611	584	678	776	630
GD	523	703	535	605	583	681	774	629
Average	521	703	536	611	582	681	774	

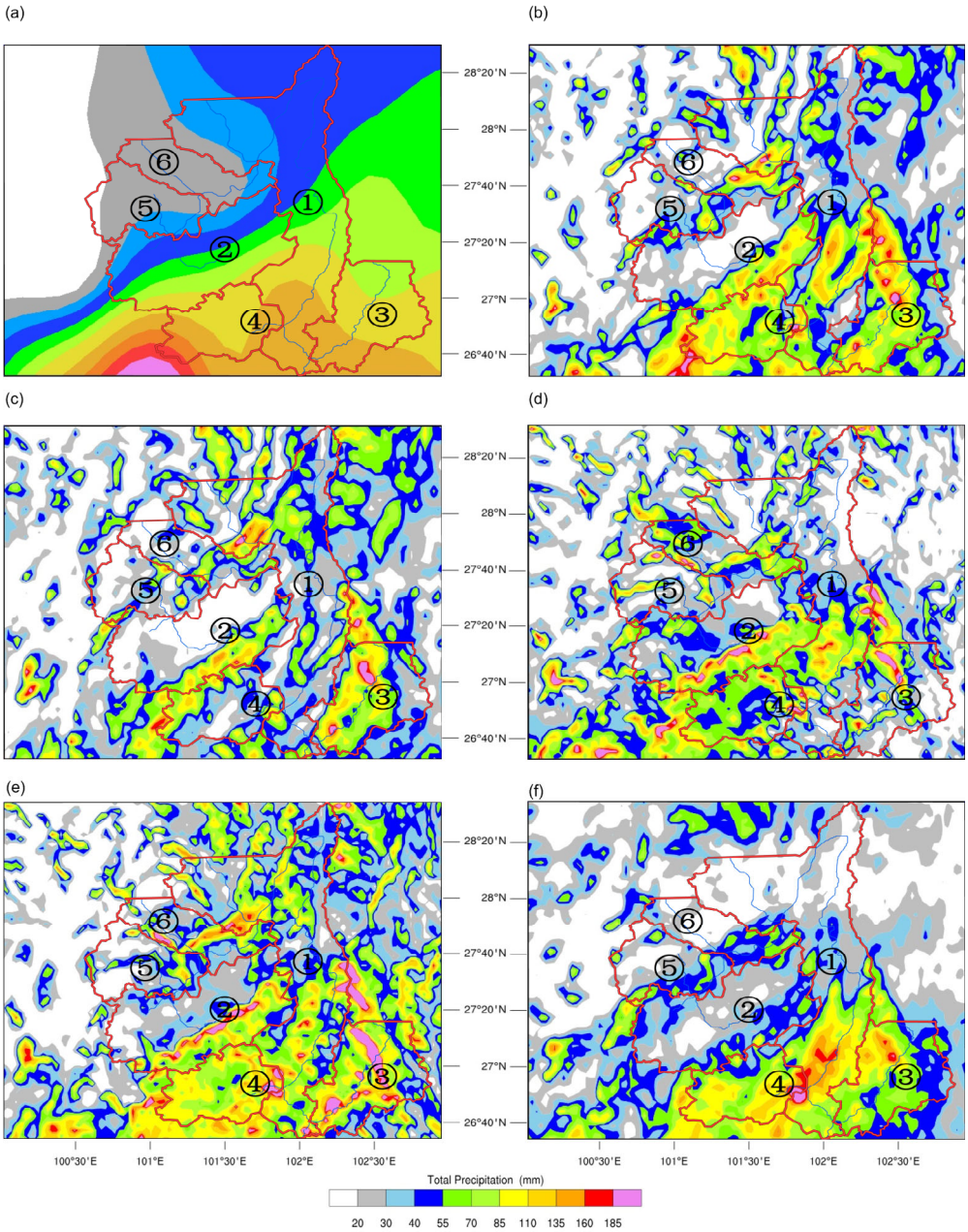

Fig. 3 Total precipitation amounts of Event A for (a) the observed precipitation, and the simulations obtained with the following MPS and CPS: (b) WSM3 & GD, (c) WSM3 & BMJ, (d) Ferrier & KF, (e) Ferrier & GD, and (f) NTH & GD. ①-⑥ are the same as those shown in Fig. 2

observed maximum precipitation. The accumulation precipitation field of WSM3 & BMJ (Fig. 3c) was much like that simulated by the WSM3 & GD scheme, but its precipitation amount was less than that simulated by the WSM3 & GD scheme and it did not reproduce the maximum precipitation in the southwest border of the study area. The precipitation provided by the Ferrier & KF (Fig. 3d) and Ferrier & GD (Fig. 3e) showed the dispersion characteristics in some small areas and the intensive precipitation field of Ferrier & GD was much larger than that simulated by the Ferrier & KF. The zones with the heavy precipitation (up to 185 mm) in the simulation result of NTH & GD (Fig. 3f) were much more centralized than the other scheme combinations, but the observed heavy precipitation center shown in the Fig. 3a was

not simulated by NTH & GD. These five selected scheme combinations all provided several heavy precipitation zones that did not exist in Fig. 3a. This could be partly caused by the simulation deviation or the sparse observation stations.

In the simulation of Event A, each combination of the MPS and CPS provided different precipitation amounts in the study area (Fig. 4). The scheme combination of Ferrier & GD simulated about 105% of the observed amount, and it was the only one that provided more precipitation than the observed precipitation across the study area (the last column in Fig. 4). All the other four schemes provided less precipitation than the observed precipitation: 87% of the observed amount by WSM3 & GD, 74% by WSM3 & BMJ, 85% by Ferrier & KF, and 82% by NTH & GD. Among all the five scheme combinations, the 105% of precipitation amount produced by the Ferrier & GD is the closest to the observed precipitation. The sub-basins with the observed precipitation amounts in ascending order were respectively sub6 (29 mm), sub5 (32 mm), sub1 (52 mm), sub2 (55 mm), sub3 (100 mm), and sub4 (127 mm), and the number of the schemes which simulated more precipitation amounts than the observations were respectively 3, 2, 2, 1, 0, and 0. This indicated that the WRF model had the tendency to underestimate the heavy precipitation amount and overestimate the light precipitation amount.

As shown in Fig. 5, WSM3 & GD had the least RMSE of 10.3 mm over the study area, followed by WSM3 & BMJ with an RMSE of 10.6 mm. The NTH & GD scheme had the greatest error of 12 mm. Hence, WSM3 & GD simulated the precipitation amount and distribution most accurately in the five scheme combinations across the study area. However, the WSM3 & GD scheme simulated a 13% less precipitation amount than the observed precipitation (Fig. 4). During Event A, most of the precipitation (127 mm) fell on sub4. The WSM3 & GD scheme and Ferrier & GD scheme simulated only 69% of the observed precipitation amount on sub4, but the result was much better than those of the other three schemes (Fig. 4). Ferrier & KF and NTH & GD provided almost the same precipitation amounts for sub4: 55% and 57% of the observed total precipitation. Their RMSE scores were also about the same: 20 mm for the Ferrier & KF scheme and 20 mm for the NTH & GD scheme. The WSM3 & BMJ scheme and WSM3 & GD scheme had the two lowest RMSE values (19 mm and 15 mm) across sub4. The lower RMSE values over the study

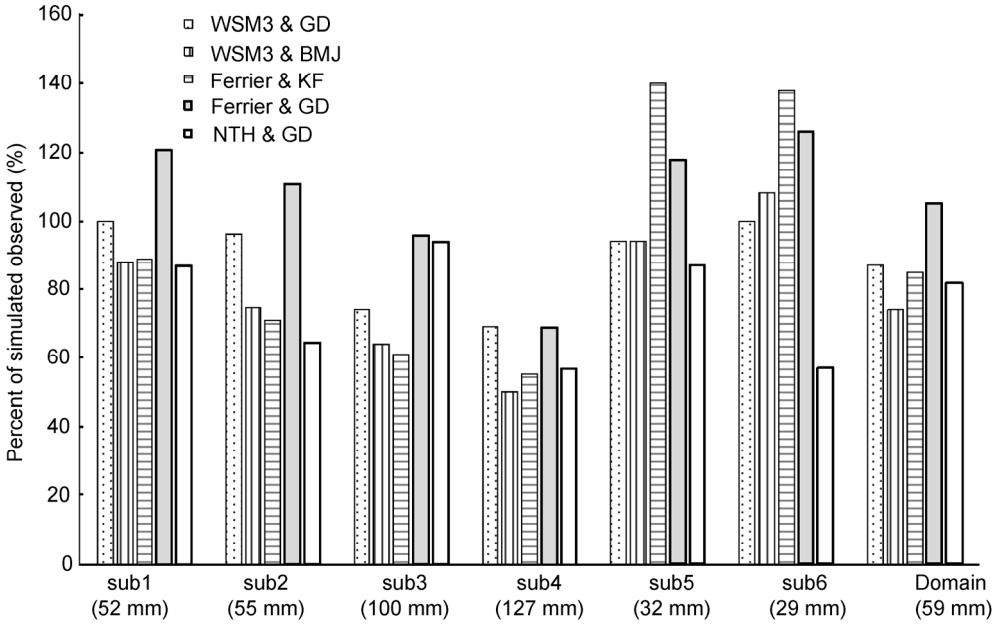

Fig. 4 Percent simulated precipitation observed for Event A at each sub-basin under the following simulation combination of MPS and CPS: WSM3 & GD, WSM3 & BMJ, Ferrier & KF, Ferrier & GD, and NTH & GD. The total precipitation amounts observed in each sub-basin are recorded in parentheses

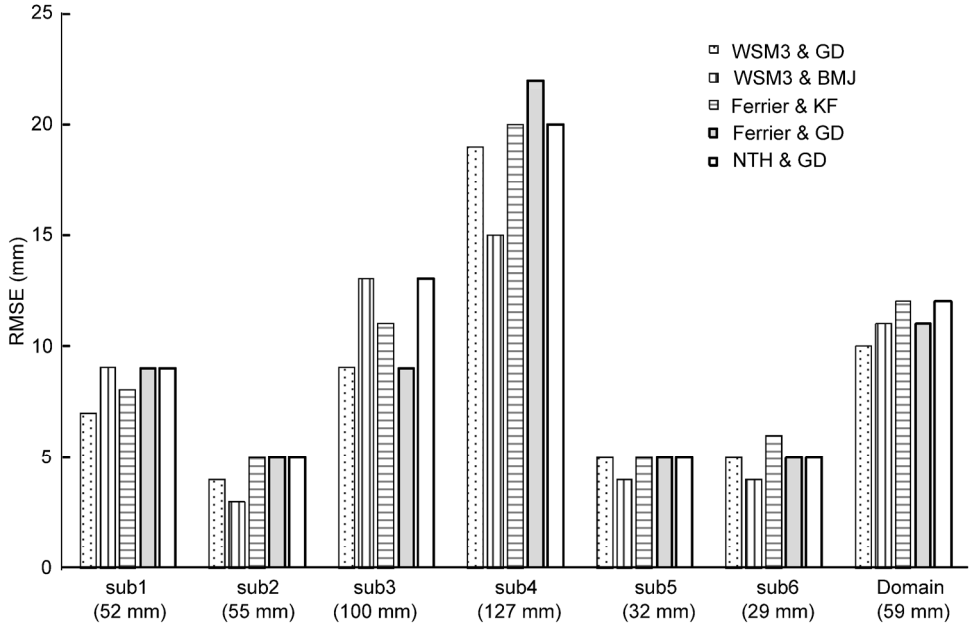

Fig. 5 RMSE values for Event A at each sub-basin obtained with the following MPS and CPS: WSM3 &GD, WSM3 &BMJ, Ferrier &KF, Ferrier &GD, and NTH &GD. The total precipitation amounts observed in each sub-basin and the study area are recorded in parentheses

area and the closer precipitation amount over sub4 (most precipitation fell on it) all indicate that the WSM3 & GD scheme and WSM3 & BMJ scheme can simulate the storm more accurately than the other three combinations, which were also proved to be the two most accurate combinations in the other sub-basins (sub1, sub2, sub5, and sub6).

Table 6 shows the results of the observation point evaluation and computational efficiency evaluation at the rainfall thresholds of 10 mm, 15 mm, and 25 mm. The flood only can be predicted on the condition that the heavy precipitation is successfully detected. Thus, we used the index of the POD to make the initial selection among the scheme combinations. In this study, we focused on the scheme combinations whose POD values exceeded 0.6 at all three thresholds. The table gives similar results as the total precipitation evaluation that the WSM3 & GD performed as well. Since the WSM3 & GD scheme and the Ferrier & GD scheme simulated more precipitation than the other scheme combinations, their POD and BIAS scores would be higher than those of other scheme combinations, as shown in Table 3. However, except for the more simulated precipitation, the WSM3 & GD was different from Ferrier & GD. The WSM3 & GD had a low FAR at three different thresholds (0.11 at 10 mm, 0.10 at 15 mm, and 0.11 at 25 mm), and had higher ET scores (0.50 at 10 mm, 0.53 at 15 mm, and 0.56 at 25 mm) than Ferrier & GD (0.49 at 10 mm, 0.4 at 15 mm, and 0.56 at 25 mm) due to their WSM3 & GD scheme's low FAR values. The FAR value of the Ferrier & GD scheme was higher than those of the other scheme combinations, indicating that the scheme combination of Ferrier & GD was falsely simulating more precipitation although it performed well in the total precipitation amount simulation across some sub-basins (Fig. 4). The WSM3 & BMJ scheme had the lowest FAR listed in the table (0.07 and 0.08), but this scheme lost its accuracy at the level of 25 mm (the POD was lower than 0.6). At the highest threshold of 25 mm, the WSM3 & GD scheme had the highest ET score, indicating that the scheme simulated heavy precipitation more accurately than other schemes in the evaluation across the observation stations. Besides simulating the precipitation accurately, the WSM3 & GD performed so well in computational efficiency that it consumed the second least time (535 min) to complete the 7-d simulation including the 1-d spin-up time. Table 6 also shows that the time consumption was mainly determined by the MPS. The NTH scheme was the most complicated, and its

computational efficiency was correspondingly the lowest: it consumed the longest time (774 min) to complete the simulation of Event A.

4.2 Event B

When evaluating the performance of the WRF model simulation for Event B, it was found that all the schemes except Kessler & * (* means KF, BMJ, and GD) were able to simulate the event accurately. The observed precipitation amount for the study area was 79 mm in 4 d. As shown in Table 7, 16 out of 21 schemes simulated the precipitation amount between 59 mm (74.6%) and 118 mm (150%). The RMSE values (Table 8) of different schemes (except Kessler & *) were only slightly different from each other, just like the evaluation result of Event A. Thus, this section will skip the detail discussion of the evaluation of the total precipitation over the river basin and go directly to the evaluation of observation point and computational efficiency.

The evaluation results of the observation point and computational efficiency are listed in Table 9. Table 9 is very long due to the good performance of different schemes on POD values. Like Event A,

Table 6 POD (higher than 0.6), FAR, BIAS, ET scores and time cost of Event A simulated by different schemes for three precipitation thresholds

MPS	CPS	Threshold (mm)	POD	FAR	BIAS	ET	Time cost (min)
Lin	KF	10	0.66	0.14	0.77	0.45	701
WSM3	KF	10	0.74	0.15	0.86	0.51	540
		15	0.70	0.13	0.80	0.53	
		25	0.66	0.15	0.77	0.52	
	BMJ	10	0.75	0.07	0.81	0.59	533
		15	0.69	0.08	0.75	0.55	
	GD	10	0.69	0.11	0.78	0.50	535
		15	0.68	0.10	0.75	0.53	
		25	0.67	0.11	0.75	0.56	
WSM5	GD	10	0.69	0.23	0.90	0.41	605
		15	0.64	0.18	0.78	0.44	
		25	0.61	0.18	0.74	0.47	
Ferrier	KF	10	0.69	0.16	0.83	0.46	579
	BMJ	10	0.65	0.15	0.76	0.44	584
	GD	10	0.78	0.20	0.97	0.49	583
		15	0.65	0.25	0.87	0.40	
		25	0.72	0.17	0.87	0.56	
NTH	GD	10	0.66	0.20	0.82	0.41	774

Table 7 Percent simulation of observed (%) of 21 model runs for Event B with seven different MPS and three different CPS

CPS	Percent simulation of observed (%)							Average
	Kessler	Lin	WSM3	WSM5	Ferrier	WSM6	NTH	
KF	2.0	99.8	95.0	74.6	112.1	81.3	49.6	73.5
BMJ	2.7	150.0	103.8	102.8	128.9	108.5	114.4	101.6
GD	35.4	66.6	80.0	86.2	97.2	89.4	114.9	81.4
Average	13.4	105.5	92.8	87.9	112.8	93.1	93.0	

Table 8 RMSE (mm) of 21 model runs for Event B with seven different MPS and three different CPS

CPS	RMSE							Average
	Kessler	Lin	WSM3	WSM5	Ferrier	WSM6	NTH	
KF	33.3	19.5	20.2	15.0	18.7	15.1	16.9	19.8
BMJ	33.0	19.4	18.9	14.6	20.4	14.5	15.3	19.4
GD	27.2	14.3	15.4	14.9	18.9	15.2	18.7	17.8
Average	31.1	17.8	18.2	14.8	19.3	14.9	17.0	

Table 9 POD (higher than 0.6), FAR, BIAS, ET scores and time cost of Event B simulated by different schemes for three precipitation thresholds

MPS	CPS	Threshold (mm)	POD	FAR	BIAS	ET	Time cost (min)
Lin	KF	10	0.69	0.05	0.73	0.29	486
		15	0.66	0.12	0.75	0.27	
		25	0.67	0.21	0.85	0.36	
	BMJ	10	0.89	0.12	1.01	0.35	484
		15	0.86	0.14	1.00	0.42	
		25	0.83	0.25	1.11	0.42	
	GD	10	0.74	0.03	0.77	0.36	485
		15	0.64	0.05	0.68	0.32	
		25	0.56	0.05	0.59	0.39	
WSM3	KF	10	0.69	0.09	0.76	0.24	382
		15	0.68	0.12	0.76	0.28	
	BMJ	10	0.72	0.11	0.81	0.22	380
		15	0.73	0.13	0.84	0.30	
	GD	10	0.74	0.06	0.78	0.36	378
		15	0.70	0.05	0.74	0.38	
		25	0.66	0.14	0.77	0.41	
WSM5	KF	10	0.78	0.06	0.83	0.37	435
		15	0.68	0.09	0.75	0.32	
	BMJ	10	0.84	0.08	0.91	0.39	434
		15	0.80	0.13	0.92	0.37	
		25	0.70	0.21	0.89	0.38	
	GD	10	0.78	0.05	0.83	0.38	435
		15	0.70	0.1	0.77	0.32	
		25	0.65	0.11	0.73	0.43	
Ferrier	KF	10	0.78	0.06	0.83	0.36	412
		15	0.76	0.11	0.86	0.36	
		25	0.74	0.21	0.94	0.41	
	BMJ	10	0.80	0.1	0.89	0.3	416
		15	0.79	0.13	0.91	0.35	
		25	0.74	0.28	1.03	0.33	
	GD	10	0.75	0.07	0.81	0.32	419
		15	0.67	0.07	0.72	0.32	
WSM6	KF	10	0.78	0.04	0.81	0.40	486
		15	0.70	0.07	0.75	0.35	
	BMJ	10	0.89	0.08	0.96	0.45	479
		15	0.82	0.12	0.93	0.40	
		25	0.75	0.22	0.97	0.40	
	GD	10	0.76	0.04	0.79	0.37	487
		15	0.68	0.06	0.72	0.35	
NTH	KF	10	0.68	0.05	0.71	0.27	562
	BMJ	10	0.90	0.08	0.98	0.47	560
		15	0.80	0.13	0.92	0.36	
		25	0.74	0.22	0.95	0.40	
	GD	10	0.82	0.09	0.90	0.35	561
		15	0.75	0.13	0.86	0.32	
		25	0.66	0.26	0.89	0.31	

we focused on the schemes that provided the POD values above the given POD value (0.6) at all the thresholds. The Lin & BMJ scheme provided the highest precipitation amount (118 mm) than the other schemes and would lead to higher POD and FAR scores. Actually, the Lin & BMJ scheme was the only scheme whose POD values exceeded 0.8 at all the three thresholds, and its average FAR was also higher than those of other schemes listed in Table 9. The Lin & GD scheme had the lowest average FAR value across the three thresholds, and the WSM3 & GD had the second lowest average FAR value and the higher POD value. In the BIAS values among different schemes, the Lin & BMJ scheme had the average BIAS value closest to 1 across the three thresholds, but its FAR values were higher than those of most of the schemes listed in the table especially at the threshold of 25 mm. The WSM6 & BMJ scheme combination had the highest average ET value across the three thresholds, and was followed by the NTH & BMJ scheme. Due to the influence of regional heavy convective precipitation, the ET scores of Event B at the threshold of 25 mm were generally lower than those of Event A. The WSM6 & BMJ scheme was the only scheme that had its ET scores higher than 0.4 at all of the three thresholds. The WSM3 & GD combination, which was the most accurate in the simulation of Event A, had a slightly lower ET score than the WSM6 & BMJ, NTH & BMJ, and Lin & BMJ schemes. However, the accuracy of the WSM3 & GD scheme was acceptable and its average value of FAR across the three thresholds was lower than most of the other schemes.

As for the time cost among the WSM6 & BMJ, NTH & BMJ, Lin & BMJ, and WSM3 & GD schemes, the former three schemes respectively consumed about 27% (about 100 min), 48% (about 200 min), and 28% (about 100 min) more time than the WSM3 & GD scheme. Taking the high-performance computing cluster into account, the absolute value of the time difference would be much greater when the simulation was run on the computers with the limited power. Therefore, the WSM6 & BMJ, NTH & BMJ, Lin & BMJ, and WSM3 & GD schemes were the acceptable scheme combinations. Furthermore, if the computation resources are limited, it is recommended to choose the WSM3 & GD scheme due to its high computational efficiency and acceptable accuracy, especially in the operational flood forecasting.

4.3 Event C

For hydrologic applications, a damaging flood can be caused by intense precipitation in a small area, which should receive greater attention and must be taken into account in our research. Event C was added to have an example of a shorter and regional rainfall that caused disasters. It was very different from Event A and Event B in relation to the precipitation amount. Event C had only one major storm from northeast to southwest. Thus, its total precipitation amount was lower than those of Event A and Event B. However, the study of Event C can better verify the use of the WRF model for reproducing a single storm in the study area. Besides, in order to evaluate the capability to simulate the rainfall progress from the non-rain status (below 20 mm/d) to heavy rainfall then to the non-rain status, two days before the storm and one day after the storm were add into the consideration for the simulation of Event C. According to the daily observed data, there was no rain in 40 stations out of 51 total stations, and only one station reached 6-mm precipitation on June 25, 2006. On next day, June 26, 2006, there was some precipitation observed by the stations, but the observed daily precipitation from 80% of the stations was lower than 15 mm, except for the Zuosuo Station, which received 43.7 mm of precipitation, which could be caused by the local weather system.

The total precipitation for Event C which fell on the study area was 55 mm, and the performance of the WRF model for simulating the total amount is shown in Table 10. The MPS of Kessler again lost its accuracy, which might be caused by its simple description of the precipitation process and the complex topography of the study area. Similar to what we did in Event A we obtained the top five scheme combinations from Tables 10 and 11. The results were as follows: WSM3 & GD, WSM3 & KF, NTH & KF, WSM6 & KF, and WSM5 & BMJ.

The WSM3 & GD scheme performed as well as it did in Event A and Event B. It successfully reproduced the rainfall progress of the single storm. Fig. 6 shows the daily precipitation simulated by the WSM3 & GD scheme from June 25 to June 30, 2006. There is almost no rain (below 20 mm/d) on June 25 (Fig. 6a)

Table 10 Percent simulation of observed (%) of 21 model runs for Event C with seven different MPS and three different CPS

CPS	Percent simulation of observed (%)							Average
	Kessler	Lin	WSM3	WSM5	Ferrier	WSM6	NTH	
KF	5.5	62.0	83.4	71.2	82.4	85.3	97.6	69.6
BMJ	8.1	75.5	120.1	109.3	139.3	74.7	117.4	92.1
GD	3.6	66.3	86.1	78.1	52.2	80.9	66.2	61.9
Average	5.7	67.9	96.5	86.2	91.3	80.3	93.7	

Table 11 RMSE (mm) of 21 model runs for Event C with seven different MPS and three different CPS

CPS	RMSE							Average
	Kessler	Lin	WSM3	WSM5	Ferrier	WSM6	NTH	
KF	22.5	11.0	10.9	11.4	12.2	11.2	11.3	12.9
BMJ	22.2	12.3	11.1	11.4	14.2	11.0	12.0	13.5
GD	22.8	11.1	10.0	11.6	11.4	12.1	10.6	12.8
Average	22.5	11.5	10.7	11.5	12.6	11.4	11.3	

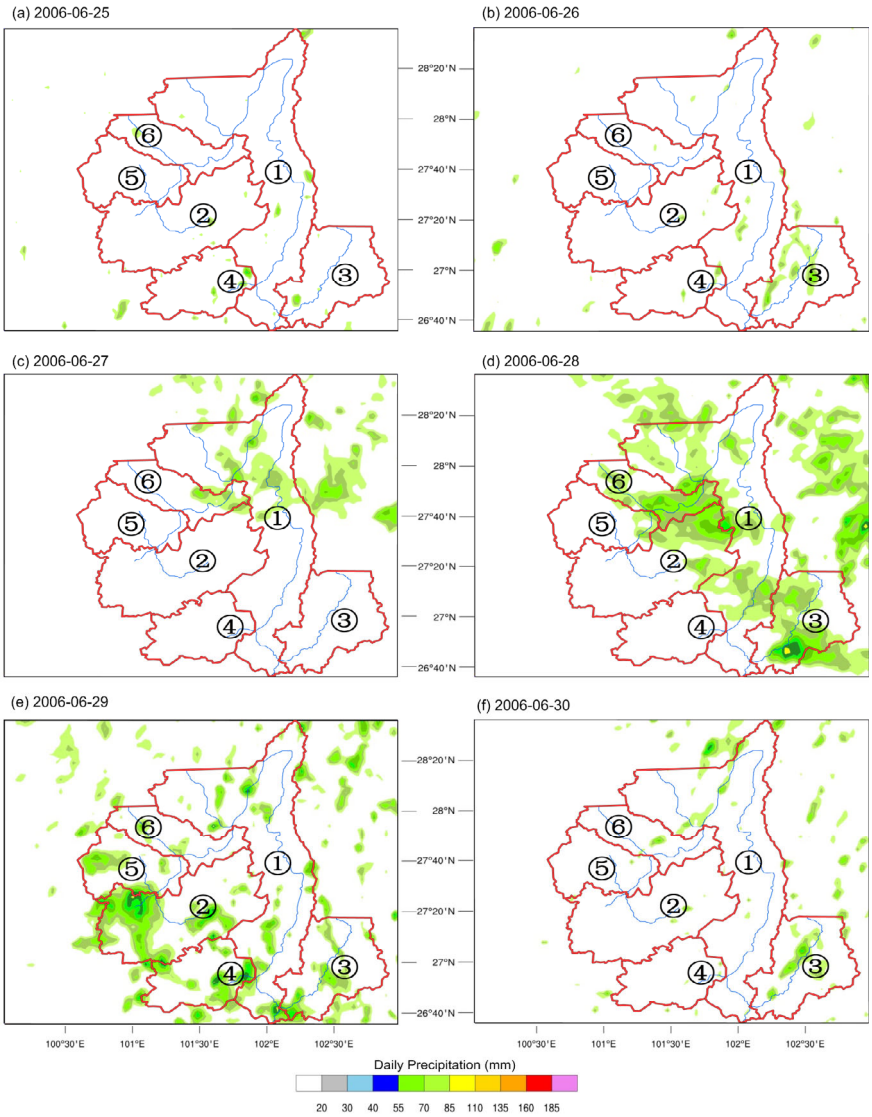

Fig. 6 Simulated daily precipitation amount distribution of WSM3 & GD for Event C in the period from two days before the single storm to one day after the storm. ①-⑥ are the same as those shown in Fig. 2

and June 26 (Fig. 6b). The heavy precipitation over a large area of the northeast of the study area occurred on June 27 (Fig. 6c). Then, the rainfall became much more intensive on June 28 (Fig. 6d), and the precipitation area was larger than it was one day previous. Fig. 6e shows that the precipitation intensity and the rainfall areas were decreased when the rainfall was moving from northeast to southwest. In Fig. 6f, the non-rain result indicates that the heavy precipitation was over on June 30, 2006.

Figs. 7 and 8 demonstrate the performance of the total precipitation and RMSE of the top five scheme combinations over 6 sub-basins and the whole study area. As shown in Fig. 7, the precipitation produced

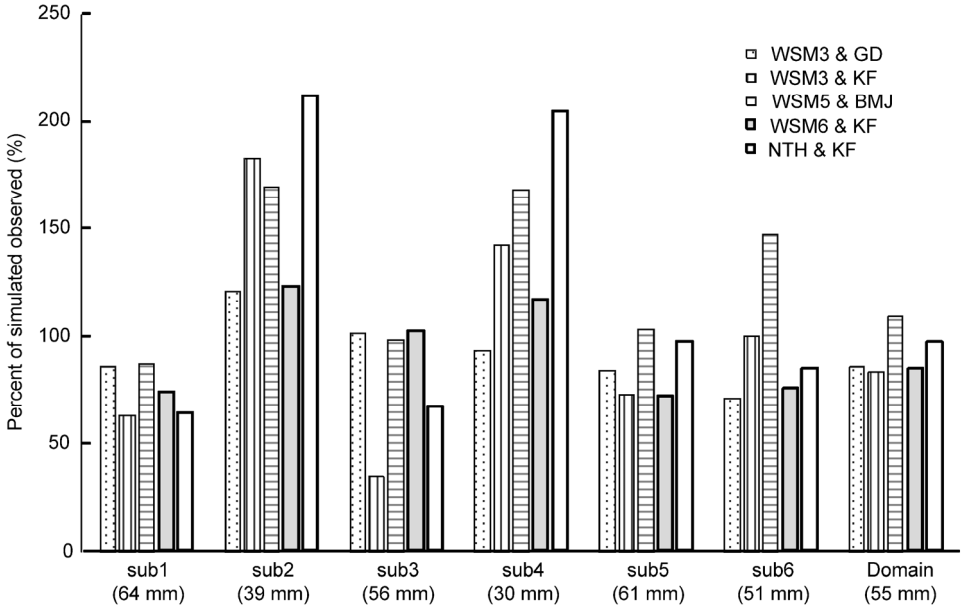

Fig. 7 Percent of the simulated precipitation accounting for the observed precipitation for Event C at each sub-basin under the following simulation combination of MPS and CPS: WSM3 & GD, WSM3 & KF, WSM5 & BMJ, WSM6 & KF, and NTH & KF. The total precipitation amount observed in each sub-basin and the study area are recorded in parentheses

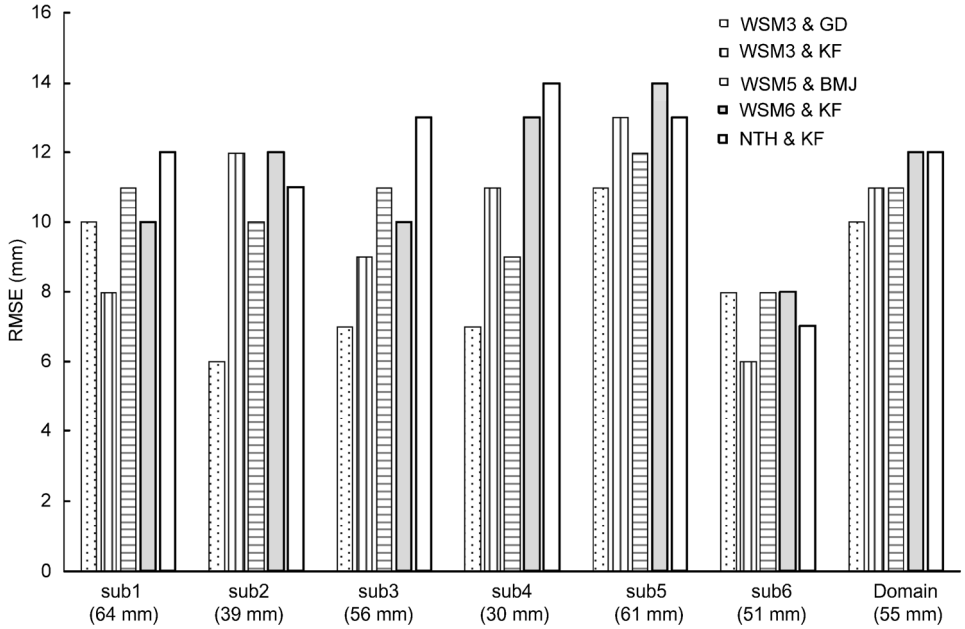

Fig. 8 RMSE values for Event C at each sub-basin obtained with the following MPS and CPS: WSM3 & GD, WSM3 & KF, WSM5 & BMJ, WSM6 & KF, and NTH & KF. The total precipitation amount observed in each sub-basin and the study area are recorded in parentheses

by the NTH & KF scheme combination is the closest to the observed precipitation across the study area (about 97%). The WSM5 & BMJ scheme was the only scheme combination that overestimated the precipitation amount in the study area, 109% of the observed precipitation amount, which was the second closest to the observed precipitation amount. The WSM3 & GD scheme and WSM3 & KF scheme performed similarly, respectively providing 86% and 83% of the observed precipitation amounts over the study area. However, the RMSE value of the WSM3 & GD scheme was 1 mm less than that of WSM3 & KF scheme due to the instable performance of the WSM3 & KF scheme across the sub-basins.

As shown in Fig. 8, the simulation results of the WSM3 & GD scheme had the lowest RMSE among all the five scheme combinations across the study area. The sub1 basin not only received the most precipitation (64 mm) during the storm, but also encountered the heaviest rainfall intensity, 63.7 mm/d, which was observed at the Jinhe Station. Due to the heavy precipitation in sub1, all the schemes underestimated the precipitation amount. Although WSM5 & BMJ and WSM3 & GD simulated only 87% and 86% of the observed precipitation amount, they simulated more precipitation than any other scheme for sub1. The scheme of WSM6 & KF provided the next highest precipitation amount, 74% of the observed precipitation amount.

The average RMSE across the five scheme combinations in sub5 was the highest among the sub-basins, indicating that the performance of the WRF model for sub5 was the worst in the six sub-basins. The simulation result of the WSM3 & GD scheme combination for sub5 gave the lowest RMSE value. However, according to Fig. 7, the scheme of WSM3 & GD was not the best one for the precipitation amount in sub5. This may be caused by the systematical precipitation underestimation of the scheme of WSM3 & GD, but the underestimated amount was not very significant. The precipitation in sub2 was only 39 mm, and all the schemes overestimated the precipitation amount. This overestimation for light rainfall was consistent with the results of Event A in this study.

Fig. 7 shows that the WSM3 & GD scheme provided 14% less precipitation than the observed precipitation across the study area. It was not the best scheme to simulate the total precipitation in the study area, but it had the lowest RMSE value (10 mm) among all the schemes. Thus, for Event C, the WSM3 & GD scheme and the WSM5 & BMJ scheme generally provided precipitation amounts and distribution more accurately than other schemes.

Table 12 shows the results of the observation point evaluation and computational efficiency evaluation at the rainfall thresholds of 10 mm, 15 mm, and 25 mm. Like the analysis of Event A and Event B, Table 12 only lists the rows with the POD value above 0.6. Table 12 shares some similar results with the evaluation in Tables 6 and 9: the schemes of WSM3 & GD, WSM5 & BMJ, and NTH & KF are included. The WSM3 & BMJ scheme combination had the highest ET (0.54) at a threshold of 25 mm, but its ET was the lowest (0.26) at a threshold of 10 mm, indicating the instability of this scheme combination. The WSM3 & GD scheme combination had the second highest ET (0.52) at a threshold of 25 mm, and its ET values at the thresholds of 10 mm and 15 mm were the highest in Table 12. As shown in Fig. 7, the

Table 12 POD (higher than 0.6), FAR, BIAS, ET scores and time cost of Event C simulated by different schemes for three precipitation thresholds

MPS	CPS	Threshold (mm)	POD	FAR	BIAS	ET	Time cost (min)
Lin	BMJ	25	0.65	0.14	0.76	0.52	671
WSM3	BMJ	10	0.72	0.36	1.11	0.26	532
		15	0.66	0.37	1.03	0.31	
		25	0.78	0.26	1.05	0.54	
	GD	10	0.61	0.17	0.67	0.32	535
		15	0.62	0.10	0.69	0.47	
		25	0.65	0.14	0.76	0.52	
WSM5	BMJ	25	0.73	0.31	1.05	0.47	602
Ferrier	BMJ	15	0.67	0.35	1.03	0.33	575
		25	0.70	0.46	1.30	0.33	
NTH	KF	25	0.65	0.29	0.92	0.43	779
	BMJ	25	0.70	0.28	0.97	0.47	781

WSM5 & BMJ scheme often overestimates the precipitation, thus leading to high values of POD, FAR, and BIAS. The advantages of the WSM3 & GD scheme in simulating Event C are obvious in Table 12, and the WSM3 & GD scheme performs stably at all three thresholds with low FAR values and high POD and ET values. In addition, the computing efficiency of the WSM3 & GD scheme is higher than most of the other schemes. It takes only 535 min to simulate Event C (7 d including 1-d spin-up time).

5 Summary and conclusions

The aim of this study is twofold: to evaluate the capability of the WRF model to simulate the heavy precipitation in the downstream area of the Yalong River Basin before applying it in the prediction of the basin flood and to find out the optimum combinations of MPS and CPS with a relatively high computational efficiency in the study area. The Yalong River Basin is an important electric power generation basin in China. However, no systematic evaluation or verification of a WRF model for heavy precipitation simulation has been previously made for this region. The results in this paper will be significant for flood forecasting and the reservoir operations in the Yalong River Basin.

We used the WRF model with seven different MPS and three CPS to simulate three historic heavy precipitation events in the downstream area of the Yalong River Basin. Thus, 63 model runs were conducted to better examine different performances of the MPS and CPS by comparing the simulations of the 3-km resolution model with available rain gauge observations. Eyeball analysis was taken for the top five scheme combinations that performed well in the total precipitation amount production and RMSE comparison in the study area. It depicted that the WRF model could reproduce the total precipitation distribution, although the location and amount of precipitation varied among different model runs. The evaluation showed that the schemes often underestimated the heavy precipitation exceeding 50 mm/d in the river basin which was similar to the underestimation of the WRF model noted by Zangl (2007) and Milbrandt and Yau (2001). The results of RMSE across the whole study area and sub-basins indicated that the heavier rainfall was much more difficult to be simulated than moderate rainfall, especially for the regional convective precipitation. Such simulation results were consistent with previous results of Event A and Event B.

Evaluations of all combinations of schemes for the three events showed that the WSM3 & GD combination provided a compromised result between computational efficiency and computational accuracy for the prediction of heavy precipitation. The WSM3 & GD scheme provided the most accurate simulations of Event A and Event C. Its performance was also very good in the simulation for Event B with the highest computational efficiency. According to the comparison results of the 24-h accumulated rainfall between the WRF model outputs and rain gauge observations for Event B, the simulation results by the Lin & GD scheme combination were slightly better than the WSM3 & GD scheme in simulating the heavy rainfall. However, its computing time was much longer than that of the WSM3 & GD scheme, and the simulation performance of the Lin & GD scheme was not consistently good for Event A or Event C. Therefore, our study suggests that the WSM3 &GD scheme combination is the optimum one with consistently stable performance for all of the three events in the study area with low FAR and high POD and ET scores.

Event C was added to have an example of a shorter and regional rainfall that caused disasters. The WRF model with the WSM3 & GD scheme successfully simulated the progress of the storm events from the non-rain status (below 20 mm/d) to heavy precipitation and then to the non-rain status again. Moreover, the scheme combination of WSM3 & GD also showed its strength in station evaluation and computational efficiency evaluation.

We can conclude that the WRF model is capable of simulating heavy precipitation events with high spatial resolution in the downstream area of the Yalong River Basin. Furthermore, the scheme combination of WSM3 and GD holds a stable performance in the accuracy and computation efficiency for the heavy precipitation prediction. This finding is very important for the runoff simulation and forecast in the Yalong River Basin, especially when the computation resources are limited, because the outputs of the NWP models with a relatively long lead time can be used as valuable inputs of the hydrologic models to predict floods.

We have to point out that we make no real criteria about how the shorter computation time would

offset higher accuracy. This is mainly because the computation time is related to the performance of the computers. If the researchers or forecasters own a high performance cluster, they may not be concerned about the computing efficiency of the schemes. Thus, the precise criteria are difficult to establish, and we only use the computation time as an important reference when selecting schemes from those with an acceptable accuracy. However, this study does give some suggestions and selects the scheme combinations with stable performance in the accuracy and computation efficiency, which will be useful to our further studies or other researchers when they conduct relative studies in the downstream area of the Yalong River Basin.

References

Alam, M.M., 2014. Impact of cloud microphysics and cumulus parameterization on simulation of heavy rainfall event during 7-9 October 2007 over Bangladesh. *Journal of Earth System Science*, **123**(2):259-279. [doi:10.1007/s12040-013-0401-0]

Benedetti, A., Lopez, P., Moreau, E., *et al.*, 2005. Verification of TMI-adjusted rainfall analyses of tropical cyclones at ECMWF using TRMM precipitation radar. *Journal of Applied Meteorology*, **44**(11):1677-1690. [doi:10.1175/JAM2300.1]

Betts, A.K., Miller, M.J., 1986. A new convective adjustment scheme. Part II: single column tests using GATE wave, BOMEX, ATEX and arctic air-mass data sets. *Quarterly Journal of the Royal Meteorological Society*, **112**(473):693-709. [doi:10.1002/qj.49711247308]

Chandrasekar, R., Balaji, C., 2012. Sensitivity of tropical cyclone Jal simulations to physics parameterizations. *Journal of Earth System Science*, **121**(4):923-946. [doi:10.1007/s12040-012-0212-8]

Cossu, F., Hocke, K., 2013. Influence of microphysical schemes on atmospheric water in the Weather Research and Forecasting model. *Geoscientific Model Development Discussions*, **6**(3):4563-4601. [doi:10.5194/gmdd-6-4563-2013]

Cressman, G.P., 1959. An operational objective analysis system. *Monthly Weather Review*, **87**(10):367-374. [doi:10.1175/1520-0493(1959)087<0367:AOOAS>2.0.CO;2]

Dodla, V.B.R., Ratna, S.B., 2010. Mesoscale characteristic and prediction of an unusual extreme heavy precipitation event over India using a high resolution mesoscale model. *Atmospheric Research*, **95**:255-269. [doi:10.1016/j.atmosres.2009.10.004]

Dodla, V.B.R., Desamsetti, S., 2014. Multi-physics ensemble prediction of tropical cyclone movement over Bay of Bengal. *Natural Hazards*, **70**(1):883-902. [doi:10.1007/s11069-013-0852-2]

Done, J., Davis, C.A., Weisman, M., 2004. The next generation of NWP: explicit forecasts of convection using the weather research and forecasting (WRF) model. *Atmospheric Science Letter*, **5**(6):110-117. [doi:10.1002/asl.72]

Evans, J.P., Ekström, M., Ji, F., 2012. Evaluating the performance of a WRF physics ensemble over South-East Australia. *Climate Dynamics*, **39**(6):1241-1258. [doi:10.1007/s00382-011-1244-5]

Ferrier, B.S., Jin, Y., Lin, Y., *et al.*, 2002. Implementation of a new grid-scale cloud and precipitation scheme in the NCEP Eta Model. 19th Conf. on Weather Analysis and Forecasting 15th Conf. on Numerical Weather Prediction, San Antonio. American Meteorological Society, USA, p.280-283.

Fiori, E., Parodi, A., Siccardi, F., 2011. Uncertainty in prediction of deep moist convective progresses: turbulence parameterizations, microphysics and grid-scale effects. *Atmospheric Research*, **100**(4):447-456. [doi:10.1016/j.atmosres.2010.10.003]

Fritsch, J.M., Chappell, C.F., 1980. Numerical prediction of convectively driven mesoscale pressure systems. Part I: convective parameterization. *Journal of the Atmospheric Sciences*, **37**(8):1722-1733. [doi:10.1175/1520-0469(1980)037<1722:NPOCDM>2.0.CO;2]

Grell, G.A., Devenyi, D., 2002. A generalized approach to parameterizing convection combining ensemble and data assimilation techniques. *Geophysical Research Letters*, **29**(14):1693-1696. [doi:10.1029/2002GL015311]

Hong, S.Y., Lim, J.O.J., 2006. The WRF single-moment 6-class microphysics scheme (WSM6). *Korean Meteorological Social*, **42**(2):129-151.

Hong, S.Y., Lee, J.W., 2009. Assessment of the WRF model in reproducing a flash-flood heavy rainfall event over Korea. *Atmospheric Research*, **93**(4):818-831. [doi:10.1016/j.atmosres.2009.03.015]

Hong, S.Y., Dudhia, J., Chen, S.H., 2004. A revised approach to ice microphysical processes for the bulk parameterization of clouds and precipitation. *Monthly Weather Review*, **132**(1):103-120. [doi:10.1175/1520-0493(2004)132<0103:ARATIM>2.0.CO;2]

Jasper, K., Kaufmann, P., 2003. Coupled runoff simulations as validation tools for atmospheric models at the regional scale. *Quarterly Journal of The Royal Meteorological Society*, **129**(588):673-693. [doi:10.1256/qj.02.26]

Jia, R.X., Hou, X.L., Liu, Y., 2004. Hydropower exploitation in Sichuan province. *Resources and Environment in the Yangtze Basin*, **13**(5):438-443 (in Chinese).

Kain, J.S., 2004. The Kain-Fritsch convective parameterization: an update. *Journal of Applied Meteorology*, **43**(1):170-181. [doi:10.1175/1520-0450(2004)043<0170:TKCPAU>2.0.CO;2]

Kain, J.S., Fritsch, J.M., 1990. A one-dimensional entraining/detraining plume model and its application in convection parameterization. *Journal of the Atmospheric Sciences*, **47**(23):2784-2802. [doi:10.1175/1520-0469(1990)047<2784:AODEPM>2.0.CO;2]

Kerkhoven, E., Gan, T.Y., Shiiba, M., *et al.*, 2006. A comparison of cumulus parameterization schemes in a numerical weather prediction model for a monsoon rainfall event. *Hydrological Processes*, **20**(9):1961-1978. [doi:10.1002/hyp.5967]

Kessler, E., 1995. On the continuity and distribution of water

substance in atmospheric circulations. *Atmospheric Research*, **38**(1-4):109-145. [doi:10.1016/0169-8095(94)00090-Z]

Lin, Y.L., Farley, R.D., Orville, H.D., 1983. Bulk parameterization of the snow field in a cloud model. *Journal of Climate and Applied Meteorology*, **22**(6):1065-1092. [doi:10.1175/1520-0450(1983)022<1065:BPOTSF>2.0.CO;2]

Litta, A.J., Mahanty, U.C., Das, S., *et al.*, 2012. Numerical simulation of severe local storms over east India using WRF-NMM mesoscale model. *Atmospheric Research*, **116**:161-184. [doi:10.1016/j.atmosres.2012.04.015]

Mastrangelo, D., Horvath, K., Riccio, A., *et al.*, 2011. Mechanisms for convection development in a long-lasting heavy precipitation event over southeastern Italy. *Atmospheric Research*, **100**(4):586-602. [doi:10.1016/j.atmosres.2010.10.010]

Michalakes, J., Dudhia, J., Gill, D., *et al.*, 1999. Design of a next-generation regional weather research and forecast model. Proceedings of Eighth ECMWF Workshop on the Use of Parallel Processors in Meteorology. Towards Teracomputing, Reading, UK. World Scientific Publishing, Singapore, p.117-124.

Milbrandt, J.A., Yau, M.K., 2001. A mesoscale modeling study of the 1996 Saguenay Flood. *Monthly Weather Review*, **129**(6):1419-1440. [doi:10.1175/1520-0493(2001)129<1419:AMMSOT>2.0.CO;2]

Peng, Y., Wang, G.L., Tang, G.L., 2011. Study on reservoir operation optimization of Ertan Hydropower station considering GFS forecasted precipitation. *Science China-Technological Sciences*, **54**(S1):76-82. [doi:10.1007/s11431-011-4623-6]

Pennelly, C., Reuter, G., Flesch, T., 2014. Verification of the WRF model for simulating heavy precipitation in Alberta. *Atmospheric Research*, **135-136**:172-192. [doi:10.1016/j.atmosres.2013.09.004]

Schaefer, J.T., 1990. The critical success index as an indicator of warning skill. *Weather and Forecasting*, **5**(4):570-575. [doi:10.1175/1520-0434(1990)005<0570:TCSIAA>2.0.CO;2]

Shamim, M.A., Remesan, R., Han, D.W., *et al.*, 2012. An improved technique for global daily sunshine duration estimation using satellite imagery. *Journal of Zhejiang University-SCIENCE A (Applied Physics & Engineering)*, **13**(9):717-722. [doi:10.1631/jzus.A1100292]

Skamarock, W.C., Klemp, J.B., Dudhia, J., *et al.*, 2008. A description of the advanced research WRF version 3. NCAR Technical Note NCAR/TN-475 + STR.

Thompson, G., Rasmussen, R.M., Manning, K., 2004. Explicit forecasts of winter precipitation using an improved bulk microphysics scheme. Part I: description and sensitivity analysis. *Monthly Weather Review*, **132**(2):519-542. [doi:10.1175/1520-0493(2004)132<0519:EFOWPU>2.0.CO;2]

Tustison, B., Harris, D., Foufoula-Georgiou, E., 2001. Scale issues in verification of precipitation forecasts. *Journal of Geophysical Research: Atmospheres*, **106**(D11):11775-11784. [doi:10.1029/2001JD900066]

Wang, H.J., Yu, E.T., Yang, S., 2011. An exceptionally heavy snowfall in Northeast China: large-scale circulation anomalies and hindcast of NCAR WRF model. *Meteorology and Atmospheric Physics*, **113**(1-2):11-25. [doi:10.1007/s00703-011-0147-7]

Wang, W., Seaman, N.L., 1997. A comparison study of convective parameterization schemes in a mesoscale model. *Monthly Weather Review*, **125**(2):252-278. [doi:10.1175/1520-0493(1997)125<0252:ACSOCP>2.0.CO;2]

Wicker, L.J., Wilhelmson, R.B., 1995. Simulation and analysis of tornado development and decay within a three-dimensional supercell thunder storm. *Journal of the Atmospheric Sciences*, **52**(15):2675-2703. [doi:10.1175/1520-0469(1995)052<2675:SAAOTD>2.0.CO;2]

Zangl, G., 2007. Interaction between dynamics and cloud microphysics in orographic precipitation enhancement: a high-resolution modeling study of two north alpine heavy precipitation events. *Monthly Weather Review*, **135**(8):2817-2840. [doi:10.1175/MWR3445.1]

Zhou, H.C., Zhang, Y., Tang, G.L., 2009. Study on medium and long term runoff forecasting for Ertan hydropower station. *Water Resources and Power*, **27**(1):5-9 (in Chinese).

中文概要

题　目：数值天气预报模式对雅砻江下游强降水预报能力检验研究

目　的：检验数值天气预报模式（WRF）在雅砻江下游对强降水的预报能力，并找出表现最优的参数化方案组合。

创新点：首次针对雅砻江流域检验 WRF 模式对强降水的预报能力，并加入了计算时间作为评价的重要参考。

方　法：通过三场强降水事件，利用七种常用的云微物理参数化方案（Kessler，Lin *et al.* (Lin)，Single-Moment 3-class (WSM3)，Single-Moment 5-class (WSM5)，Ferrier，Single-Moment 6-class (WSM6)，和 New Thompson *et al.* (NTH)）和 3 种积云对流参数化方案（Kain-Fritsch (KF), Betts-Miller-Janjic (BMJ)和 Grell-Devenyi (GD)）的组合，对 WRF 模式在雅砻江下游的降水预报能力进行检验。为了评价 WRF 模式的预报能力，引入探测率（POD），空报率（FAR），BIAS 和公平预报评分（ETS），对比不同方案组合的降水空间分布和站点预报的有效性。同时，均方根误差（RMSE）等指标被用来评价面雨量预报的精确性。除常规评价外，还将计算时间作为方案评价的重要参考，在满足精度需求的前提下优先选择计算效率高的方案组合。

结　论：1. WRF 模式能够适用于雅砻江下游强降水预报；2. WSM3 以及 GD 参数化方案组合的表现最为有效和稳定。

关键词：WRF 模式；雅砻江流域；降水模拟；积云对流参数化方案；云微物理参数化方案